Front Instabilities Can Reverse Desertification

Cristian Fernandez-Oto,[1,2] Omer Tzuk,[3] and Ehud Meron[1,3]
[1]Department of Solar Energy and Environmental Physics, BIDR, Ben-Gurion University of the Negev, Sede Boqer Campus, 84990 Israel
[2]Complex Systems Group, Facultad de Ingenieria y Ciencias Aplicadas, Universidad de los Andes, Av. Mon. Alvaro del Portillo 12.455 Santiago, Chile
[3]Physics Department, Ben-Gurion University of the Negev, Beer-Sheva 84105, Israel

(Received 9 October 2018; revised manuscript received 26 November 2018; published 30 January 2019)

Degradation processes in living systems often take place gradually by front propagation. An important context of such processes is loss of biological productivity in drylands or desertification. Using a dryland-vegetation model, we analyze the stability and dynamics of desertification fronts, identify linear and nonlinear front instabilities, and highlight the significance of these instabilities in inducing self-recovery. The results are based on the derivation and analysis of a universal amplitude equation for pattern-forming living systems for which nonuniform instabilities cannot emerge from the nonviable (zero) state. The results may therefore be applicable to other contexts of animate matter where degradation processes occur by front propagation.

DOI: 10.1103/PhysRevLett.122.048101

Front propagation is a driver of state transitions and functional changes in various contexts of living systems. Gene-expression fronts drive embryo development [1–3], fronts of cell proliferation and migration drive cancer [4,5], species invasion drives community-structure changes and loss of ecosystem function [6], and fronts of plant mortality drive desertification [7]. In all contexts, local processes at the front zone gradually induce global transitions to new asymptotic states, the nature of which depends on three main aspects of front dynamics [8,9]. The first pertains to the dynamics of a single front, and to whether it propagates or is pinned [10]; front propagation gradually shifts the system from one stable state to another, while front pinning can result in a variety of stable hybrid states involving spatial mixtures of the two alternative states [11,12]. The second aspect relates to the interactions that develop as two fronts approach one another. Repulsive front interactions can prevent the coalescence of growing domains [13,14] and, thereby render gradual state shifts incomplete [9]. The third aspect of front dynamics is front instabilities that involve a reversal in the direction of front propagation [15–17]. These front instabilities are of particular interest because of the potential they hold for reversing degradation processes.

Two types of front instabilities can be distinguished: longitudinal instabilities, involving structural front changes in the direction of front propagation, and transverse instabilities in which the structural changes are along the front line [18]. Transverse instabilities have been studied in models of bacterial growth [19,20] and tumor growth [4,21], while longitudinal instabilities have been studied in a model of actin polymerization [17], and in several ecological contexts, including a three-species Lotka-Volterra model [22] and a dryland vegetation model [9]. These studies have mostly been concerned with unraveling instability mechanisms, paying little attention to functional aspects of front instabilities, such as reversing degradation processes.

In this Letter we identify linear and nonlinear transverse instabilities [23] of desertification fronts, and study their utilization in inducing *self-recovery* of degraded landscapes. While providing new insights about the challenging problem of reversing desertification processes, which are of world-wide concern [7,24], our study also highlights universal aspects that might be relevant to other contexts of degrading living systems.

Our starting point is a dryland vegetation model introduced by Gilad *et al.* [8,25,26], which captures remarkably well a wide range of vegetation pattern-formation phenomena [27–31]. We consider here a simplified version of the model, relevant to sandy soil for which overland water flow is insignificant [30]. The simplified model consists of two state variables, the areal densities of the above-ground vegetation biomass $b(\mathbf{r},t)$ and of the soil-water content $w(\mathbf{r},t)$. Expressed in terms of nondimensional state variables and parameters, the model reads [26,30]

$$\begin{aligned}\partial_t b &= bw(1+\eta b)^2(1-b) - b + \nabla^2 b,\\ \partial_t w &= p - \frac{nw}{1+\rho b} - \gamma b w(1+\eta b)^2 + \delta\nabla^2 w,\end{aligned} \tag{1}$$

where η is a measure of the root-to-shoot ratio, $\nabla^2 b$ is a biomass-diffusion term representing seed dispersal, p is the precipitation rate, n is the evaporation rate, γ is the water-uptake rate, ρ quantifies reduced evaporation

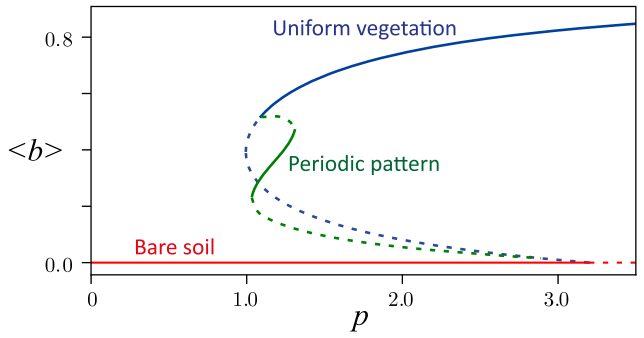

FIG. 1. Bifurcation diagram of stationary solutions of Eqs. (1). The vertical axis represents the spatial biomass average, while the horizontal axis represents the precipitation (rainfall) rate. Solid (dashed) lines represent stable (unstable) solutions. Note the existence of a wide bistability range of bare soil and uniform vegetation, and of a tristability range of these states with a periodic pattern. Parameters: $n = 3.2$, $\gamma = 0.5$, $\rho = 1.0$, $\eta = 3.5$, and $\delta = 300$. Dimensional precipitation and biomass density are $P = 400p$ [mm/year] and $B = 0.5b$ [kg/m^2] (see the Supplemental Material [32] for more details).

due to shading, $\nabla^2 w$ describes soil-water diffusion, and δ is the ratio of soil-water diffusivity to biomass diffusivity (seed dispersal rate). More details about the model and its dimensional parameters are described in the Supplemental Material [32].

The dynamical-system context we consider here is illustrated in the bifurcation diagram shown in Fig. 1. A bare-soil (zero biomass) state loses stability to a uniform vegetation state in a subcritical uniform instability, as the precipitation exceeds a threshold value, that results in a bistability range of the two uniform states. Furthermore, a positive feedback loop between local vegetation growth and soil-water diffusion towards the growth location can result in a nonuniform instability of the uniform-vegetation state [33]. This secondary instability leads to a stationary periodic vegetation pattern [30], and a possible tristability range of bare soil, uniform vegetation, and periodic pattern [34]. Additional periodic solutions that extend to lower precipitation rates exist but are not shown [35,36]. This bifurcation structure, which follows from the model equations (1) as well as from other vegetation models [37–39], reflects the constraint that the bare-soil state cannot undergo a nonuniform instability to avoid unphysical negative biomass values. Periodic vegetation patterns, if they exist, should appear then from a nonuniform instability of the uniform-vegetation state.

Within the bistability range of the two uniform states front solutions biasymptotic to the two states exist [9]. These solutions include a desertification front that describes the expansion of bare soil into uniform vegetation. The first question we address here is whether such a front can go through a transverse instability that results in vegetation fingering and growth patterns that reverse the desertification process. In order to study a transverse instability of this kind and the factors that control it, we reduce Eq. (1) to a universal amplitude equation for the uniform mode that grows beyond the instability of the bare-soil state, and analyze front solutions of this equation in one and two spatial dimensions.

We derive the amplitude equation close to the precipitation threshold, $p = p_c = n$, at which the bare-soil state loses stability, and close to the threshold value $\eta = \eta_c = (1 + \gamma/n)/2$, above which a bistability range of bare soil and uniform vegetation develops. For simplicity we take $\rho = 0$. In the vicinity of the critical point (p_c, η_c) the amplitude of the growing uniform mode is small and we can express solutions of Eq. (1) as

$$\begin{pmatrix} b \\ w \end{pmatrix} = \begin{pmatrix} b_c \\ w_c \end{pmatrix} + \lambda \begin{pmatrix} b_1 \\ w_1 \end{pmatrix} + \lambda^2 \begin{pmatrix} b_2 \\ w_2 \end{pmatrix} + \cdots, \quad (2)$$

where $(b_c, w_c) = (0, 1)$ is the bare-soil solution at the critical point, $(b_1, w_1) = \tilde{C}(1, -\gamma/n)$ is the growing uniform eigenmode with an amplitude $\tilde{C}$, and $\lambda \ll 1$ is a small auxiliary parameter, quantifying the vicinity to the critical point as follows:

$$p - p_c \equiv \alpha = \alpha_0 \lambda^2, \qquad \eta - \eta_c \equiv \varepsilon = \varepsilon_0 \lambda, \quad (3)$$

where α_0 and ε_0 are of order unity. Using a multiple timescale analysis we find the amplitude equation

$$\partial_t C = a_1 C + a_2 C^2 - a_3 C^3 + d_1(C)\nabla^2 C - d_2(C)\nabla^4 C, \quad (4)$$

where $C = \lambda \tilde{C} = b$ and

$$a_1 = \alpha/n, \qquad a_2 = 2\varepsilon, \qquad a_3 = 3\eta_c^2,$$
$$d_1 = 1 - \gamma\delta C/n^2, \qquad d_2 = \gamma\delta^2 C/n^3. \quad (5)$$

The reader is referred to the Supplemental Material [32] for a detailed derivation of Eq. (4). Here, we motivate the structure of this equation, highlighting its universal nature for pattern-forming living systems in general for which state variables cannot assume negative values.

The first three terms on the right side of Eq. (4) constitute the normal form of an imperfect pitchfork bifurcation of a nonviable state $C = 0$ to a viable state $C = C_0 > 0$ with a bistability range of the two uniform states. The last two terms on the right side of Eq. (4) account for the spatial nature of the instabilities that the two uniform states go through subjected to the constraint $C \geq 0$, as the state variable (biomass, population density, concentration of a biochemical agent, etc.) cannot assume negative values. The requirement that the nonviable state goes through a uniform instability (to avoid negative C values), implies $d_1(0) \geq 0$ and $d_2(0) \geq 0$, and the requirement that the viable state goes through a nonuniform instability (to allow for patterns), implies $d_1(C_0) < 0$ and $d_2(C_0) > 0$. To linear

order in C this suggests a dependence of the form $d_1(C) = d_{10} - d_{11}C$, where d_{10} and d_{11} are positive constants. Furthermore, the requirement that front solutions, connecting the nonviable and viable states, do not have oscillatory tails about the nonviable state (to avoid again negative C values) implies the condition $d_2(0) < d_1(0)^2/4|a_1|$ [40]. To linear order in C this suggests a dependence of the form $d_2(C) = d_{20} + d_{21}C$, where d_{20} and d_{21} are positive constants, and $d_{20} < d_{10}^2/4|a_1|$. We thus expect the amplitude equation (4) with the above expressions for $d_1(C)$ and $d_2(C)$ to apply to pattern-forming living systems in general, including dryland ecosystems described by different models. Indeed, Eq. (4) has been obtained from a different vegetation model [41,42], and a similar equation has been derived to describe Lotka-Volterra type dynamics of a species population distributed along a niche axis [43]. Models of inanimate systems can also lead to a similar equation but with no constraints on the coefficients as described above [44].

In order to study front solutions of Eq. (4) and possible instabilities thereof we introduce a rescaled amplitude $A(\mathbf{r}, t) = 9\eta_c^2 C(\mathbf{r}, t)/4\varepsilon$ in terms of which Eq. (4) reads

$$\partial_t A = -\nu^2 A(A-1)\left(A - \frac{1}{2}\right) + \nabla^2 A + \mu A - D_1 A\nabla^2 A - D_2 A\nabla^4 A, \tag{6}$$

where $\nu^2 = 2^4\varepsilon^2/3^3\eta_c^2$, $\mu = \alpha/n + \nu^2/2$, $D_1 = 4\varepsilon\gamma\delta/9\eta_c^2 n^2$ and $D_2 = D_1\delta/n$. We consider first the special case $\mu = \delta = 0$. In this case Eq. (6) simplifies to the variational equation $A_t = -\delta V/\delta u$ where V is a double-well potential with minima of equal depth at $A = 0$ and $A = 1$—the two uniform states that describe bare soil and uniform vegetation. This case corresponds to the so-called Maxwell point at which planar front solutions biasymptotic to the two uniform states are stationary [45–47]. These solutions have the analytical form [48]

$$A_F(x - x_0) = \frac{1}{2}\left[1 - \tanh\left(\frac{\nu(x - x_0)}{2\sqrt{2}}\right)\right], \tag{7}$$

where x is the spatial coordinate normal to the front line and x_0 is the arbitrary position of the front. In the following we use Eq. (7) to identify a transverse front instability and obtain an analytical expression for its threshold.

We study the stability of planar fronts to transverse perturbations by deriving a linear relation between the normal velocity of the front, i.e., the velocity in a direction normal to the front line V_n and the front's curvature, κ [8,49]. We refer to this instability as a linear front instability. For simplicity, we consider here a circular front [50] close to the Maxwell point, of radius $r_0(t)$ that is much larger than the front width, i.e., $r_0 \gg \nu^{-1}$ or $\kappa = 1/r_0 \ll \nu$. The Laplacian operator acting on the amplitude A then simplifies to $\nabla^2 = \partial_r^2 + \kappa\partial_r$, where r is the radial coordinate and we have replaced r^{-1} by $r_0^{-1} = \kappa$, since the only place where the spatial derivatives of the amplitude A are not negligible is the front zone where $r \approx r_0$. Expressing the circular front as a perturbed planar front,

$$A(r, t) = A_F[r - r_0(t)] + W[r, r_0(t), t], \tag{8}$$

where A_F is given by Eq. (7) and W is a small correction, and employing a solvability condition associated with the existence of a marginal translational mode in a homogeneous system [8], we find the following expression for the normal front velocity $V_n = dr_0/dt$ (see the Supplemental Material [32]):

$$V_n = V_0 - F\kappa, \tag{9}$$

where

$$V_0 = \sqrt{2}\left(\frac{3\mu}{\nu} + \frac{\nu D_1}{20} - \frac{\nu^3 D_2}{56}\right), \qquad F = 1 - \frac{D_1}{2} + \frac{\nu^2 D_2}{10}.$$

The onset of a transverse front instability is determined by the condition $F = 0$ [18], which defines a threshold value δ_c of δ. For $\varepsilon \ll 1$ this threshold can be approximated by

$$\delta_c \approx \frac{9{\eta_c}^2 n^2}{2\gamma\varepsilon}. \tag{10}$$

The instability occurs as δ is increased past the threshold δ_c, that is, when soil-water diffusion is fast enough relative to biomass diffusion. This result can be understood as follows. Consider a bulge in the front line, as Fig. 2 illustrates, and the local normal velocity as compared with

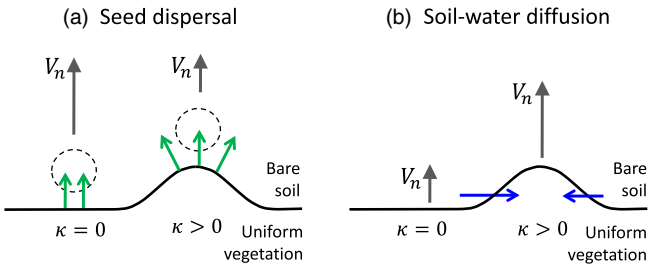

FIG. 2. Schematic illustration of diffusive processes that stabilize and destabilize a planar front. (a) Biomass diffusion (seed dispersal) acts to stabilize a planar front against the growth of an initial vegetation bulge (positive curvature) because of the smaller diffused biomass per unit area ahead of the bulge as compared with a planar front segment. (b) Soil-water diffusion has the opposite effect of destabilizing a planar front by accelerating the growth of a vegetation bulge and inhibiting vegetation growth in the bulge surroundings. This is because of water uptake in the vegetated bulge area, which creates soil-water gradients and induces soil-water diffusion from the bulge surroundings toward the bulge.

that of a planar front segment. When biomass diffusion dominates (small δ), the front velocity of a bulge will be lower than that of a planar front because of the more scattered biomass diffusion ahead of the bulge. As a result an initial bulge in a planar front will fade away in the course of time. By contrast, when soil-water diffusion dominates (large δ), the front velocity of a bulge will be higher than that of a planar front because of the enhanced water uptake by the vegetation in the bulge area, and the concomitant soil-water depletion on both sides of the bulge. The growth of small, randomly created bulges in a planar front renders such a front unstable. Note that the threshold δ_c in Eq. (10) is inversely proportional to $\varepsilon = \eta - \eta_c > 0$, and therefore has a monotonically decreasing dependence on η. This is inline with the instability mechanism described above, as higher values of the root-to-shoot ratio imply stronger water uptake by the vegetation in the bulge area and sharper soil-water gradients, which favor the instability at smaller thresholds δ_c. The analysis of the amplitude equation has been useful to get insights into the mechanism that drives the transverse front instability. This equation, however, is limited to the close vicinity of the critical point (p_c, η_c). Below, we extend our study to a wider parameter range using Eqs. (1).

The development of a transverse front instability is demonstrated numerically in Fig. 3. The initial condition corresponds to a desertification front, subjected to small transverse biomass modulations. The instability results in vegetation fingers growing into bare soil, as the normal velocity at the tip of a finger can be positive even though the velocity of the planar front is negative, $V_n = -|V_0| + |F|\kappa > 0$. Thus, a transverse front instability can reverse gradual desertification by gradually shifting an unproductive bare-soil state to a productive labyrinthine vegetation pattern that prevents further irreversible degradation processes, such as soil erosion.

Among the parameters that affect the transverse-front instability—soil-water diffusion, precipitation and evaporation rates, water uptake rate, and root-to-shoot ratio—only the latter two can be controlled in practice by the introduction of a new plant species at the front zone. Desertification processes may possibly be reversed by introducing species with sufficiently high root-to-shoot ratio or water-uptake rate so as to lower δ_c below the soil-water diffusion rate δ of the given environment, and thereby induce a transverse instability. However, there is an additional dynamical property of Eq. (1) that bears on the question of controlling desertification, namely, the tristability range of bare soil, uniform vegetation, and periodic pattern. In this range, linearly stable desertification fronts may still be unstable to *finite-amplitude* transverse modulations that drive the system to the periodic-pattern state through finger growth [23] as Fig. 4(a) and 4(b) demonstrate. This nonlinear front instability defines a range, $\delta_c > \delta > \delta_n$, where local manipulations at the front zone to induce finite-amplitude transverse modulations can reverse desertification. These manipulations may consist of periodic clearcutting, grazing, or irrigation along the

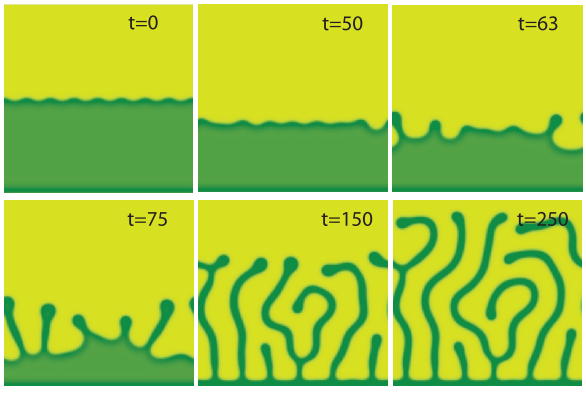

FIG. 3. Linear front instability. Numerical solutions of Eqs. (1) showing a desertification front that is unstable to a transverse sinusoidal modulation. Following a short phase in which the bare-soil domain expands into the uniform-vegetation domain, vegetation fingers develop and grow back into the bare-soil domain, as the snapshots show. Parameters: $n = 3.2$, $\gamma = 0.5$, $\rho = 1.0$, $\eta = 3.5$, $p = 1.17$, and $\delta = 300$. The time indicated in every snapshot is in units of years.

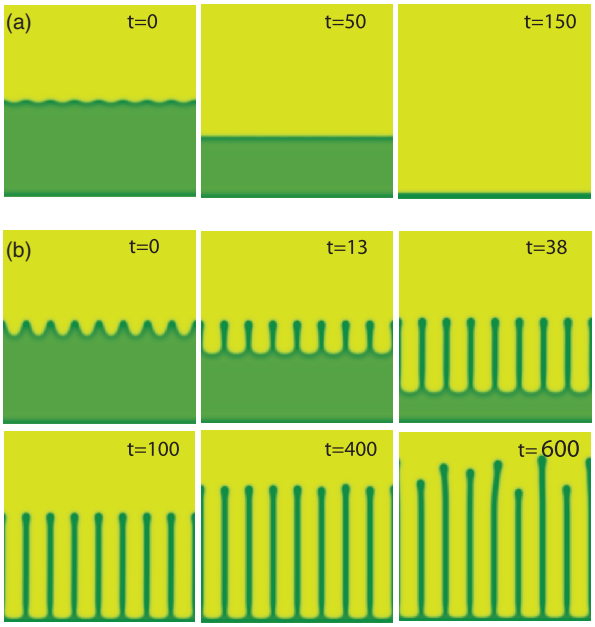

FIG. 4. Nonlinear front instability in a tristability range of Eqs. (1). (a) Snapshots showing the stability of a planar desertification front to small transverse modulation. (b) Snapshots showing the instability of the planar front to sufficiently large transverse modulations and the development of vegetation fingers that grow back into bare soil. In all simulations the same parameters were used: $n = 3.2$, $\gamma = 0.5$, $\rho = 1.0$, $\eta = 3.5$, $p = 1.15$, and $\delta = 150$. The time indicated in every snapshot is in units of years.

front line. The possible existence of a nonlinear front instability of a desertification front can be inferred from observations of domains of periodic patterns in the same region. The reversal of desertification can be accelerated by diluting the number of vegetation fingers in order to reduce the competition for water, as we demonstrate in the Supplemental Material [32]. Although a highly diluted state may be far less productive than the nondiluted state, it is still significant in maintaining the ecosystem in a reversible state. Once vast soil areas become bare, further degradation takes place, such as soil erosion and loss of soil fertility, making the desertification process highly irreversible. The recovery in a patterned state, even sparse and less productive, can prevent this additional degradation.

We focused here on dryland vegetation and desertification, but the context is more general—pattern-forming living systems having nonviable states that go through subcritical instabilities to viable states. The constraint of non-negative state variables results in an amplitude equation [Eq. (4)], which is somewhat similar to the well-studied Swift-Hohenberg equation [8,12,52], but contains nonlinear spatial-derivative terms. The universal nature of the amplitude equation derived here makes it relevant to various contexts of animate matter where typical state variables, such as population densities of organisms and concentrations of biochemical reagents, cannot assume negative values.

We thank Edgar Knobloch for a helpful discussion. The research leading to these results has received funding from the Israel Science Foundation under Grant No. 305/13. Cristian Fernandez-Oto acknowledge the financial support of FONDECYT Project No. 3170227.

[1] A. C. Oates, L. G. Morelli, and S. Ares, Development (Cambridge, U.K.) **139**, 625 (2012).
[2] A. Kicheva, M. Cohen, and J. Briscoe, Science **338**, 210 (2012).
[3] A. M. Tayar, E. Karzbrun, V. Noireaux, and R. H. Bar-Ziv, Nat. Phys. **11**, 1037 (2015).
[4] E. Khain and L. M. Sander, Phys. Rev. Lett. **96**, 188103 (2006).
[5] O. Chepizhko, C. Giampietro, E. Mastrapasqua, M. Nourazar, M. Ascagni, M. Sugni, U. Fascio, L. Leggio, C. Malinverno, G. Scita *et al.*, Proc. Natl. Acad. Sci. U.S.A. **113**, 11408 (2016).
[6] F. M. Hilker, M. A. Lewis, H. Seno, M. Langlais, and H. Malchow, Biol. Invasions **7**, 817 (2005).
[7] P. D'Odorico, A. Bhattachan, K. F. Davis, S. Ravi, and C. W. Runyan, Adv. Water Resour. **51**, 326344 (2013).
[8] E. Meron, *Nonlinear Physics of Ecosystems* (CRC Press/Taylor & Francis Group, Boca Raton, 2015).
[9] Y. R. Zelnik and E. Meron, Ecol. Indic. **94**, 544 (2018).
[10] Y. Pomeau, Physica **23D**, 3 (1986).
[11] D. J. B. Lloyd, B. Sandstede, D. Avitabile, and A. R. Champneys, SIAM J. Appl. Dyn. Syst. **7**, 1049 (2008).
[12] E. Knobloch, Annu. Rev. Condens. Matter Phys. **6**, 325 (2015).
[13] A. Hagberg and E. Meron, Nonlinearity **7**, 805 (1994).
[14] P. van Heijster, A. Doelman, T. J. Kaper, and K. Promislow, SIAM J. Appl. Dyn. Syst. **9**, 292 (2010).
[15] C. Elphick, A. Hagberg, and E. Meron, Phys. Rev. E **51**, 3052 (1995).
[16] D. Haim, G. Li, Q. Ouyang, W. D. McCormick, H. L. Swinney, A. Hagberg, and E. Meron, Phys. Rev. Lett. **77**, 190 (1996).
[17] E. Bernitt, H.-G. Dbereiner, N. S. Gov, and A. Yochelis, Nat. Commun. **8**, 15863 (2017).
[18] A. Hagberg and E. Meron, Chaos **4**, 477 (1994).
[19] H. Levine and E. Ben-Jacob, Phys. Biol. **1**, P14 (2004).
[20] C. Giverso, M. Verani, and P. Ciarletta, J. R. Soc. Interface **12**, 20141290 (2015).
[21] M. Ben Amar, C. Chatelain, and P. Ciarletta, Phys. Rev. Lett. **106**, 148101 (2011).
[22] M. Mimura and M. Tohma, Ecol. Complexity **21**, 215 (2015).
[23] A. Hagberg, A. Yochelis, H. Yizhaq, C. Elphick, L. Pismen, and E. Meron, Physica **217D**, 186 (2006).
[24] J. F. Reynolds *et al.*, Science **316**, 847 (2007).
[25] E. Gilad, J. von Hardenberg, A. Provenzale, M. Shachak, and E. Meron, Phys. Rev. Lett. **93**, 098105 (2004).
[26] E. Meron, Math. Biosci. **271**, 1 (2016).
[27] C. Valentine, J. d'Herbes, and J. Poesen, Catena **37**, 1 (1999).
[28] V. Deblauwe, N. Barbier, P. Couteron, O. Lejeune, and J. Bogaert, Global Ecol. Biogeogr. **17**, 715 (2008).
[29] S. Getzin, K. Wiegand, T. Wiegand, H. Yizhaq, J. von Hardenberg, and E. Meron, Ecography **38**, 1 (2015).
[30] Y. R. Zelnik, E. Meron, and G. Bel, Proc. Natl Acad. Sci. U.S.A. **112**, 12327 (2015).
[31] S. Getzin, H. Yizhaq, B. Bell, T. E. Erickson, A. C. Postle, I. Katra, O. Tzuk, Y. R. Zelnik, K. Wiegand, T. Wiegand *et al.*, Proc. Natl Acad. Sci. U.S.A. **113**, 3551 (2016).
[32] See Supplemental Material at http://link.aps.org/supplemental/10.1103/PhysRevLett.122.048101 for dimensional equations, derivation of the amplitude equation, derivation of the velocity-curvature relation, accelerating recovery by front dilution.
[33] E. Meron, Annu. Rev. Condens. Matter Phys. **9**, 79 (2018).
[34] Y. R. Zelnik, P. Gandhi, E. Knobloch, and E. Meron, Chaos **28**, 033609 (2018).
[35] Y. R. Zelnik, S. Kinast, H. Yizhaq, G. Bel, and E. Meron, Phil. Trans. R. Soc. A **371**, 20120358 (2013).
[36] K. Siteur, E. Siero, M. B. Eppinga, J. D. Rademacher, A. Doelman, and M. Rietkerk, Ecol. Complexity **20**, 81 (2014).
[37] R. Lefever and O. Lejeune, Bull. Math. Biol. **59**, 263 (1997).
[38] J. von Hardenberg, E. Meron, M. Shachak, and Y. Zarmi, Phys. Rev. Lett. **87**, 198101 (2001).
[39] M. Rietkerk, M. Boerlijst, F. van Langevelde, R. HilleRisLambers, J. van de Koppel, L. Kumar, H. H. T. Prins, and A. De Roos, Am. Nat. **160**, 524 (2002).

[40] This condition is obtained by considering a stationary front, calculating the eigenvalues about $C = 0$ of the spatial ordinary differential equation obtained by setting the time derivative in Eq. (4) to zero, and requiring real-valued eigenvalues.
[41] O. Lejeune and M. Tlidi, Journal of vegetation science : official organ of the International Association for Vegetation Science **10**, 201 (1999).
[42] O. Lejeune, M. Tlidi, and P. Couteron, Phys. Rev. E **66**, 010901 (2002).
[43] P. V. Paulau, D. Gomila, C. López, and E. Hernández-García, Phys. Rev. E **89**, 032724 (2014).
[44] G. Kozyreff and M. Tlidi, Chaos **17**, 037103 (2007).
[45] R. E. Goldstein, G. H. Gunaratne, L. Gil, and P. Coullet, Phys. Rev. A **43**, 6700 (1991).
[46] G. Bel, A. Hagberg, and E. Meron, Theor. Ecol. **5**, 591 (2012).
[47] C. Fernandez-Oto, M. G. Clerc, D. Escaff, and M. Tlidi, Phys. Rev. Lett. **110**, 174101 (2013).
[48] D. Escaff, C. Fernandez-Oto, M. G. Clerc, and M. Tlidi, Phys. Rev. E **91**, 022924 (2015).
[49] A. Hagberg and E. Meron, Physica **123D**, 460 (1998).
[50] A more general analysis, leading to the same velocity-curvature relation, can be obtained by transforming to a coordinate system that moves with a weakly curved front line [49,51].
[51] A. Hagberg and E. Meron, Phys. Rev. Lett. **78**, 1166 (1997).
[52] M. Cross and P. Hohenberg, Rev. Mod. Phys. **65**, 851 (1993).